Philosophical Magazine

ISSN: 1478-6435 (Print) 1478-6443 (Online) Journal homepage: http://www.tandfonline.com/loi/tphm20

Orientation relationships of Laves phase and NiAl particles in an AFA stainless steel

Geneva Trotter & Ian Baker

To cite this article: Geneva Trotter & Ian Baker (2015): Orientation relationships of Laves phase and NiAl particles in an AFA stainless steel, Philosophical Magazine, DOI: 10.1080/14786435.2015.1111529

To link to this article: http://dx.doi.org/10.1080/14786435.2015.1111529

Published online: 30 Nov 2015.

Submit your article to this journal

View related articles

View Crossmark data

Full Terms & Conditions of access and use can be found at
http://www.tandfonline.com/action/journalInformation?journalCode=tphm20

Download by: [Dartmouth College Library] **Date:** 01 December 2015, At: 05:54

Philosophical Magazine, 2015
http://dx.doi.org/10.1080/14786435.2015.1111529

Taylor & Francis
Taylor & Francis Group

Orientation relationships of Laves phase and NiAl particles in an AFA stainless steel

Geneva Trotter and Ian Baker*

Thayer School of Engineering, Dartmouth College, Hanover, NH 03755, USA

(*Received 17 June 2015; accepted 18 October 2015*)

The alumina-forming austenitic (AFA) stainless steel, Fe–20Cr–30Ni–2Nb–5Al (in at. %) was solutionized at 1250 °C in order to obtain a fully austenitic microstructure and then aged for up to 1325 h at 800 °C to precipitate the Laves phase and B2-NiAl particles typically found in AFAs. This paper describes detailed analyses of the orientation relationships between these particles and the matrix which were determined by transmission electron microscopy. Four variants of the $(1\,1\,1)_m//(0\,0\,0\,1)_p$, $[\bar{1}\,1\,0]_m//[1\,0\,\bar{1}\,0]_p$ orientation relationship proposed by Denham and Silcock (J. Iron Steel Inst. 207 (1969) p.582) were observed for the Laves phase, and six variants of the $(1\,1\,1)_m//(0\,1\,1)_p$, $[\bar{1}\,0\,1]_m//[\overline{1}\,\overline{1}\,1]_p$ Kurdjumov–Sachs relationship were observed for the B2-NiAl phase.

Keywords: Precipitate-orientation relationship; transmission electron microscopy; austenite; intermetallics; Laves phase

Downloaded by [Dartmouth College Library] at 05:54 01 December 2015

Introduction

Alumina (Al_2O_3)-forming austenitic (AFA) stainless steels have shown potential to decrease reliance on expensive Ni-based alloys for aggressive environments in energy production and chemical processing environments [1]. AFAs use alumina as a protective oxide scale for high corrosion resistance since alumina is known to offer even better protection than chromia at high temperatures [2,3]. AFA stainless steels were in development as early as the 1970s [4] and more recently AFAs have received renewed attention for their promising materials properties [1,5–21].

Within particular grades of AFAs, the influence of precipitate phases on creep strength is complex. A wide variety of creep strengths can be obtained with relatively small changes in alloying elements. Phases that are beneficial in some AFAs cause decreased creep strength in others. The Laves phase, for example, having shown long-term stability at high temperatures [7,9,15,22], has been investigated for its ability to act as a strengthener [7,9,18,20,21]. Along with the Laves phase, the role of B2-NiAl particles in AFAs has been investigated. B2-NiAl particles have been shown to act as strengtheners in room temperature tensile tests in AFA alloys, but have not shown any strengthening effect at 750 °C due to the brittle-to-ductile transition common to B2 intermetallic compounds [15]. The B2 particles support the formation of the alumina layer in AFAs by acting as an Al reservoir [13,15].

*Corresponding author. Email: Ian.Baker@dartmouth.edu

© 2015 Taylor & Francis

Downloaded by [Dartmouth College Library] at 05:54 01 December 2015

The Laves phase has an AB_2 stoichiometry and can exist as three closely related structures C14, C15 and C36. C15 ($MgCu_2$, $Fd\bar{3}m$) is the cubic form of the Laves phase, C14 is a hexagonal structure ($MgZn_2$, $P6_3/mmc$) and C36 which is also hexagonal ($MgNi_2$, $P6_3/mmc$). Identification of the specific structure prevalent for an alloy system can vary with composition and heat treatment [23]. In some instances different structures are present in a given alloy [24] or one structure transforms into another [25–27]. Two crystal structures can often be present in a single particle [25,28]. The C14-type Fe_2Nb Laves phase that has been observed in studies of AFAs and scanning electron microscope (SEM) images typically has a plate-like morphology.

The B2-NiAl phase has CsCl crystal structure, space group $Pm\bar{3}m$. B2 particles are spherical in some materials such as precipitation-hardenable martensitic stainless steels [29] and have also shown plate-like morphology in Fe–Ni–Cr–Al (FNCA) alloys [30,31]. There are few observations of diffraction patterns with the Laves phase being compared along with its parent matrix. While extensive work has been done recently by Bhowmik and coworkers [32–37] and Kumar and coworkers in the past [24,25,38–40] in understanding Cr_2Ta Laves phase structures and polymorphs, observed in Cr–Ta alloys, the Fe_2Nb Laves phase has received comparatively very little attention. As noted in [23] there are not many clear diffraction patterns in the literature depicting the Laves phase in stainless steel. In this study, both Laves phase and B2-NiAl particles were formed from ageing a solutionized, single-phase f.c.c. matrix of Fe–20Cr–30Ni–2Nb–5Al, with the objective of determining the crystallographic relation between the f.c.c. matrix and the Laves phase and B2-NiAl precipitates via transmission electron microscope (TEM) observations.

Experimental

Fe–20Cr–30Ni–2Nb–5Al (at. %) was cast into 15.24-cm long, 2.54-cm diameter ingots by vacuum arc-melting followed by drop casting into a copper crucible, courtesy of Dr Easo P. George. After casting the alloy was homogenized for 24 h at 1250 °C. The alloy was then aged at 800 °C for up to 1325 h [18]. An FEI XL30 SEM operated at 15 kV was used to observe microstructural features. Samples for the SEM were ground using silicon carbide papers up to 1200 grit and polished to a mirror finish using 0.3 and 0.05 μm alumina powder in water. Specimens for TEM observation were cut into rectangular bars that were milled into 3-mm diameter cylinders. The cylinders were cut into 3-mm discs and polished to ~150 μm thick. The thin foils were then twin jet electropolished in a solution of 25% nitric acid in methanol using a Struers Tenupol 5 at a voltage of 11 V and current of 100 mA at −20 °C. Microstructural examination of the specimens was performed using a Tecnai F20 FEG TEM operated at an accelerating voltage of 200 keV and equipped with an energy dispersive spectrometer (EDS).

Experimental selected area diffraction patterns (SADPs) were simulated using CrystalMaker® 9.1.3 and SingleCrystal® 2.3.1 software. The lattice parameters used to simulate SAD patterns for the matrix ($a = 0.361$ nm), Laves phase particles ($a = 0.482$ nm, $c = 0.784$ nm) and NiAl particles ($a = 0.289$ nm) were determined from X-ray diffraction from [18]. The value for the Laves phase is comparable to that obtained for $(Fe, Cr, Ni)_2(Nb, Si)$ Laves particles ($a = 0.476$ nm and $c = 0.786$ nm) in a Fe–15Cr–15Ni–Nb (wt. %) austenitic stainless steel that had additions of Si and other alloying elements [41]. Without 2 wt. % niobium the alloy had a matrix lattice parameter of $a = 0.3549$ nm, and with niobium the austenite lattice expanded to 0.3556 nm

[41]. A study of deformation behaviour in an AFA steel used a similar lattice parameter of 0.361 nm for the f.c.c. matrix [20]. The Laves lattice parameter noted in this study also falls within the range found in a study of Fe–Ni–Nb, by Takeyama et al. [42] and Denham and Silcock [43]. The lattice parameter of stoichiometric B2-NiAl was reported to be 0.28864 nm [44] and the lattice parameters of Ni-(42-55)Al has been shown to fall in the range of 0.287–0.289 nm [45].

Results and discussion

Overview of precipitates

Laves phase and B2-NiAl particles in Fe–20Cr–30Ni–2Nb–5Al typically appear to grow in distinct directions [7,18,19]. Figure 1 shows SEM backscattered electron (BSE) images of Fe–20Cr–30Ni–2Nb–5Al after both solution treatment and a series of ageing treatments at 800 °C. In Figure 1(a), the alloy shows no evidence of precipitation and is single-phase f.c.c. After ageing at 800 °C for 24 h Laves phase particles showing bright contrast have precipitated uniformly in the matrix with a few (dark) B2-NiAl particles present (Figure 1(b)). Three lines are drawn on the image parallel to the long axis of the particles and a circle is drawn for the particles that appear to project out of the image. The Laves phase particles appear to grow in only four directions. In Figure 1(c), the BSE allows one to clearly see the larger, darker contrast B2-NiAl particles that are present at 240 h, which in some instances have grown to be much larger than the Laves phase precipitates. In Figure 1(d), unlike at earlier times, after ageing at 1325 h all NiAl particles that are visible in the matrix are much larger than the Laves phase particles in the matrix. Four lines are drawn on the image parallel to the NiAl particles, suggesting there are at least four growth directions for the NiAl particles.

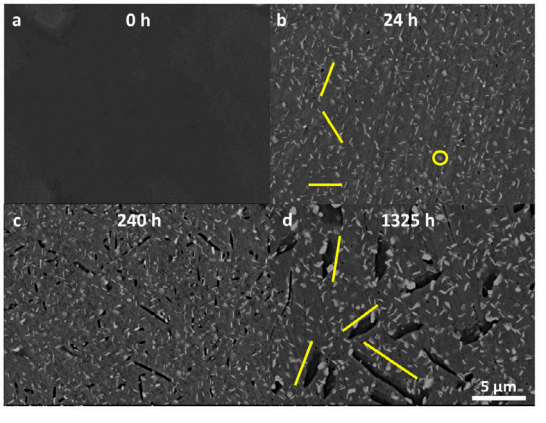

Figure 1. (colour online) BSE images showing Fe–20Cr–30Ni–2Nb–5Al matrix after (a) solution treatment, and after subsequent ageing at 800 °C for (b) 24 h lines superimposed along the long axis of the Laves phase particles and a circle representing particles that appear to project from the image; (c) 240 h; and (d) 1325 h with lines superimposed on the images are along the long axis of the NiAl particles.

Downloaded by [Dartmouth College Library] at 05:54 01 December 2015

Downloaded by [Dartmouth College Library] at 05:54 01 December 2015

TEM–EDS results from the particles and matrix are presented in Table 1. The average matrix composition after ageing at 800 °C for 1325 h has decreased amounts of Cr, Ni and Nb, and increased amounts of Fe and Al as compared to the nominal alloy composition. The B2-NiAl particles primarily consist of Ni (49.9 at. %) and Al (38.1 at. %) with substantial amounts of Fe (9.2 at. %). The values obtained for the B2-NiAl ((Ni, Fe)Al) particles are consistent with the B2-NiAl particle composition observed in a martensitic precipitation hardenable steel where atom probe data also showed a lower Al content and an incorporation of Fe while the Ni content was at 50 at. % [46]. The Fe_2Nb ((Fe, Cr, Ni)$_2$Nb) Laves phase particles consisted primarily of Fe (40.3 at. %), Cr (14.2 at. %), Ni (15.4 at. %) and Nb (28 at. %). Similar compositions for Fe_2Nb Laves particles were observed by the author [19] and in other works [41,42,47,48]. For example, in a study of the alloy Fe–15Nb–40Ni (at. %) the Laves phase had a composition of Fe-27 at. % Nb-33 at. % Ni [47] and a study of Fe–16.2Cr–14.3Ni–1.2Nb (at. %) [41] described (Fe, Ni, Cr)$_2$(Nb, Si) particles with a composition of Fe–12.6Ni–11.3Cr–22.9Nb–6.8Si (at. %), indicating a consistency in how the 'A' and 'B' elements that contribute to the AB_2 Laves phase are proportioned.

Laves phase crystal structure and orientation relationship

There are six fundamental four-layer stacking schemes that can be combined to form Laves phase as described by Komura [49] and two four-layer schemes make up the C14 structure. The C14 phase has 12 atoms per unit cell. The stacking of the C14 structure along the (0 0 0 1) planes is similar to the …ABAB… stacking sequence observed in hcp structures [50]. There are a number of ways to describe the stacking sequence. For example, as described by Komura [49], the two layers form in the close-packed direction and follow an …AB′AB′… pattern, described as: αAαcßBßc… where αAαc represents the 'A' and ßBßc represents the 'B' [51]. Greek letters correspond to large atoms (Nb in Fe_2Nb) and Roman letters correspond to smaller atoms (Fe). Figure 2(a) shows a C14 Laves projection onto a (0 0 0 1) plane. Depending on which atoms are chosen to occupy the corner sites of a unit cell, different descriptions of the stacking constructions can be used. For example, Chen et al. [52] describes the AB_2 C14 structure with small 'B' atoms making up the corners of the unit cell (Figure 2(b)) and consisting of two blocks, B1 and B1′ containing a series of primed and unprimed planes that are twin related Figure 2(c). Figure 2(d) shows the typical representation of a C14 unit cell. Kumar and Hazzledine [24] have an alternate description of the C14 stacking sequence where large atoms occupy the corners of a unit cell (Figure 2(e)). The Laves structure is described as a construction of XY′ quadruple layers which are

Table 1. Average composition of phases observed in Fe–20Cr–30Ni–2Nb–5Al after ageing at 800 °C for 1325 h as determined by EDS (in at. %). The standard deviations from a minimum of five measurements each for the f.c.c. matrix, B2-NiAl particles and Laves phase are included.

Phase	Fe	Cr	Ni	Nb	Al
fcc	44.2 ± 0.9	19.1 ± 0.3	28.2 ± 0.2	0.8 ± 0.1	7.8 ± 1.0
B2	9.2 ± 0.6	2.2 ± 0.1	49.9 ± 3.7	0.5 ± 0.0	38.1 ± 4.3
Laves	40.3 ± 1.1	14.2 ± 0.9	15.4 ± 2.4	28.0 ± 4.7	2.1 ± 0.6

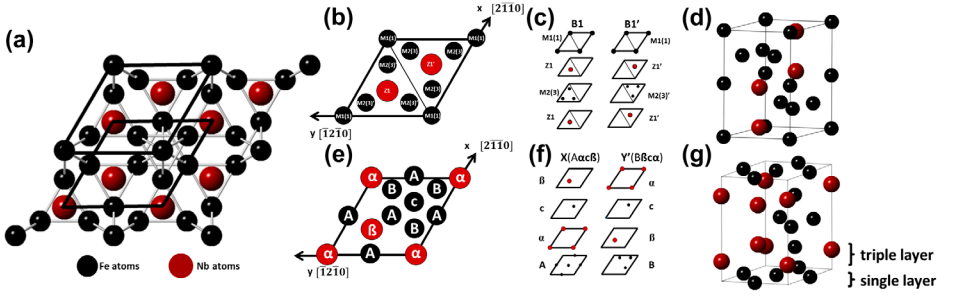

Figure 2. (colour online) (a) C14 Laves phase projection onto a (0 0 0 1) plane; (b) The atomic positions of Fe (black circles) and Nb (red circles) of a unit cell projected on (0 0 0 1) where small 'B' atoms in the AB_2 C14 Laves structure occupy the corner sites of the unit cell as described by Chen et al [52]; (c) The stacking sequence consisting of B1 and B1′ four-layer blocks; (d) Fe_2Nb unit cell; (e) The atomic positions of Fe and Nb in a unit cell projected on (0 0 0 1) in the XY′ stacking sequence as described by Kumar and Hazzledine [24]; (f) The X (Aαcß)Y′(Bßcα) stacking sequence layers; (g) Fe_2Nb unit cell showing the single and triple layers that make up a quadruple layer.

made up of alternating triple and single layers (Figure 2(f)). Each triple layer is ¼ of the thickness of the quadruple layer and contains one atom per unit cell layer. The single layer contains three small atoms (Figure 2(g)).

The orientation relationship between the Laves phase particles and the matrix was investigated via tilting experiments in the TEM. A bright-field image of a hexagonally shaped Laves phase precipitate in the f.c.c. matrix is shown in Figure 3(a). Figure 3(b) and (c) show kikuchi patterns taken from the matrix and a Laves phase precipitate, respectively. Figure 3(d) shows a SADP of the precipitate and matrix. A schematic representation of the SADP with indexing is shown in Figure 3(e). The six-fold symmetry in Figure 3(e) is consistent with the basal plane of the Laves phase (hexagonal (C14), $P6_3/mmc$). The Laves phase precipitate was oriented along the [0 0 0 1] direction while the matrix was at [1 1 1]. Based on the diffraction patterns, and simulated results, the orientation relationship between the Fe_2Nb precipitate and the austenite matrix for this particle was confirmed to be:

$$(0\,0\,0\,1)Fe_2Nb//(1\,1\,1)_\gamma$$

$$[1\,0\,\bar{1}\,0]Fe_2Nb//[\bar{1}\,1\,0]_\gamma$$

This is the relationship observed by Denham and Silcock [43] for Laves phase precipitates in an f.c.c. alloy with Fe, Cr, Ni, Nb and other minor constituents, and also in a Fe–16.2Cr–14.3Ni–1.2Nb (at. %) alloy with minor alloying additions [41]. The Laves phase precipitate has the close-packed basal (0 0 0 1) planes parallel to the close-packed (1 1 1) matrix planes that exhibit three-fold symmetry and a hexagonal pattern. While many particles were observed with the above orientation, a number of variants were observed, which was expected from the observation of particles SEM images (Figure 1).

In Figure 4(a), a TEM bright-field image of an elongated Laves particle is shown. A SADP of the particle is shown in Figure 4(b) and the simulated matrix/Laves particle

Downloaded by [Dartmouth College Library] at 05:54 01 December 2015

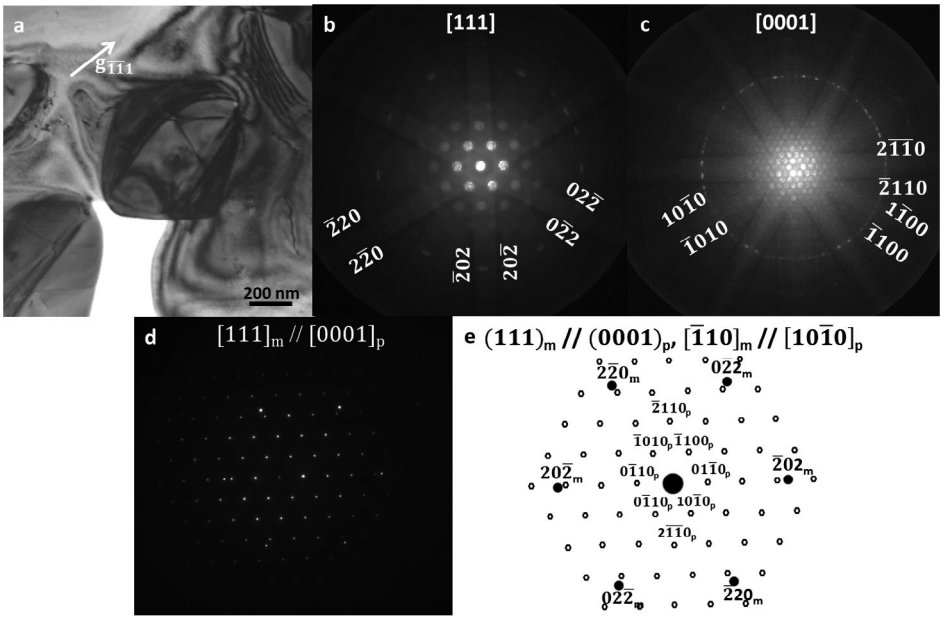

Figure 3. (a) A bright-field image of a hexagonal Laves phase precipitate; (b) Kikuchi pattern of the matrix [1 1 1] zone axis when (c) the C14 Laves precipitate was at the [0 0 0 1] zone axis. (d) selected area electron diffraction pattern from both the Laves phase particle at [0 0 0 1] and the f.c.c. matrix at [1 1 1] showing a $(1\,1\,1)_m//(0\,0\,0\,1)_p$, $[\bar{1}\,1\,0]_m//[1\,0\,\bar{1}\,0]_p$ orientation relationship. (e) Schematic representation of the orientation relationship observed in (d) with indexing.

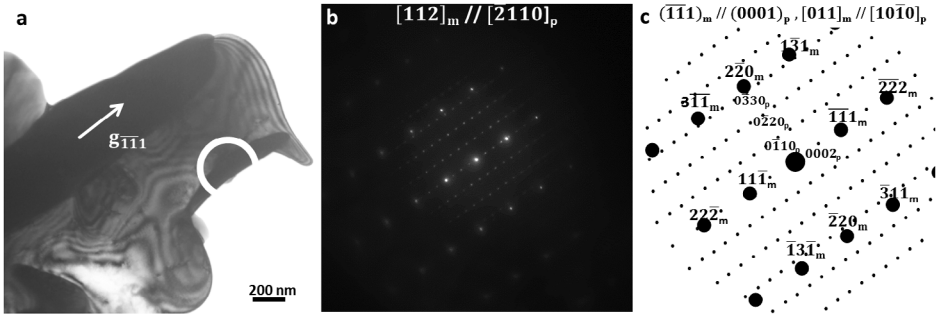

Figure 4. (a) A bright-field image showing a variant of the Laves phase; (b) selected area electron diffraction pattern from both the Laves phase particle at $[\bar{2}\,1\,1\,0]$ and the f.c.c. matrix at [1 1 2] showing a $(\overline{1\,1}\,1)_m//(0\,0\,0\,1)_p$, $[0\,1\,1]_m//[1\,0\,\bar{1}\,0]_p$ orientation relationship. (c) Schematic representation of the orientation relationship observed in (b) with indexing. The solid circles represent reflections from the matrix and the hexagons represent reflections from the Laves phase.

diffraction pattern is shown in Figure 4(c). The matrix is viewed along the [1 1 2] zone axis and the Laves phase along the $[\bar{2}\,1\,1\,0]$. This precipitate has the specific orientation of $(\overline{1\,1}\,1)_m//(0\,0\,0\,1)_p$, $[0\,1\,1]_m//[1\,0\,\bar{1}\,0]_p$.

Downloaded by [Dartmouth College Library] at 05:54 01 December 2015

Downloaded by [Dartmouth College Library] at 05:54 01 December 2015

The bright-field image in Figure 5 shows Laves phase/matrix-orientation variants. The Laves phase particles labelled with a '1' and a '2' are analysed. Laves phase particles labelled with a '(1)' or a '(2)' have the same orientation relationships of particles '1' and '2', respectively. The SADP in Figure 5(b) is taken from precipitate '1' and the SADP in Figure 5(c) is taken from precipitate '2'. In both SADPs the f.c.c. matrix is at viewed along the [1 0 1] zone axis. Figure 5(d) and (e) shows a representation of the superimposed electron diffraction patterns from both the matrix and the two particles with both particles being viewed along their $[0\,\bar{1}\,1\,0]$ zone axis. Tilting experiments and the correspondence between the image and the electron diffraction pattern of the particles, revealed that the particle whose SADP is shown in Figure 5(b) has an orientation of $(\bar{1}\,1\,1)_m//(0\,0\,0\,1)_p$, $[0\,1\,\bar{1}]_m//[1\,0\,\bar{1}\,0]_p$ and that shown in Figure 5(c) has an orientation of $(\overline{1\,1}\,1)_m//(0\,0\,0\,1)_p$, $[0\,1\,1]_m//[1\,0\,\bar{1}\,0]_p$. These particles grow along the matrix {1 1 1} planes ($(\bar{1}\,1\,1)$ in Figure 5(d) and $(\overline{1\,1}\,1)$ in Figure 5(e)). The particle shown in Figure 5(c) has the same orientation relationship as the particle presented in Figure 4. Both of these particles have similar morphologies and their long axis pointing along the same direction.

In Figure 6 a fourth variant of the orientation relationship between the matrix and the Laves phase is observed. Figure 6(a) shows a TEM bright-field image with an elongated Laves phase precipitate labelled '1'. The particle labelled '(1)' was also found to have the same orientation as particle '1'. This precipitate is at an angle to the two other

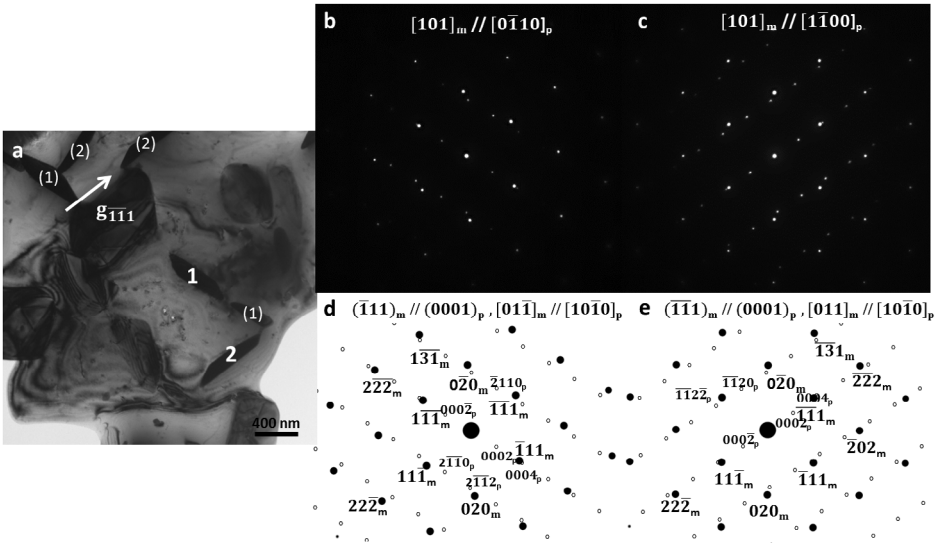

Figure 5. (a) A bright-field image showing multiple variants of the Laves phase. Particles labelled with '1' and '2' are shown in the analysis. Particles marked with '(1)' and '(2)' were found to have the same orientation relationship as '1' and '2', respectively; (b) selected area electron diffraction pattern from Laves phase particle '1' at $[0\,\bar{1}\,1\,0]$ and the f.c.c. matrix at [1 0 1] showing a $(\bar{1}\,1\,1)_m//(0\,0\,0\,1)_p$, $[0\,1\,\bar{1}]_m//[1\,0\,\bar{1}\,0]_p$ orientation relationship; (b) selected area electron diffraction pattern from both Laves phase particle '2' and the f.c.c. matrix at [1 0 1] showing a $(\overline{1\,1}\,1)_m//(0\,0\,0\,1)_p$, $[0\,1\,1]_m//[1\,0\,\bar{1}\,0]_p$ orientation relationship; (d and e) schematic representation of the orientation relationship observed in (b and c), respectively, with indexing.

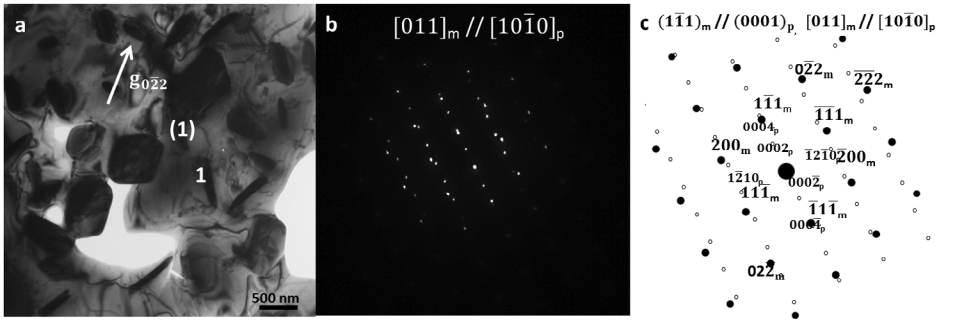

Figure 6. (a) A bright-field image showing a Laves phase precipitate variant. The particle labelled with '1' is shown in the analysis. The particles marked with '(1)' was found to have the same orientation relationship as '1'; (b) SADP of Laves particle '1' phase showing a $(1\,\bar{1}\,1)_m//(0\,0\,0\,1)_p$, $[0\,1\,1]_m//[1\,0\,\bar{1}\,0]_p$ variant; (c) Schematic representation of the orientation relationship observed in (b) with indexing.

elongated Laves phase precipitates observed in Figure 5. Figure 6(b) shows a diffraction pattern taken from particle '1' along the matrix [0 1 1] zone with the Laves phase precipitate at the $[1\,0\,\bar{1}\,0]$ zone. Figure 6(c) shows the orientation relationship $(1\,\bar{1}\,1)_m//(0\,0\,0\,1)_p$, $[0\,1\,1]_m//[1\,0\,\bar{1}\,0]_p$ for particle '1' as determined through tilting experiments. The particles were observed to grow along the matrix $(1\,\bar{1}\,1)$ plane.

In total, there were four primary variants of the Denham- and Silcock-orientation relationship observed in this study:

$$(1\,1\,1)_m//(0\,0\,0\,1)_p,\ [\bar{1}\,1\,0]_m//[1\,0\,\bar{1}\,0]_p, \tag{1}$$

$$(\bar{1}\,1\,1)_m//(0\,0\,0\,1)_p,\ [0\,1\,\bar{1}]_m//[1\,0\,\bar{1}\,0]_p, \tag{2}$$

$$(1\,\bar{1}\,1)_m//(0\,0\,0\,1)_p,\ [0\,1\,1]_m//[1\,0\,\bar{1}\,0]_p, \tag{3}$$

Table 2. Twelve variants of the Denham- and Silcock-orientation relationship.

Variant number	Plane parallel	Direction parallel
V1	$(1\,1\,1)_m//(0\,0\,0\,1)_p$	$[\bar{1}\,1\,0]_m//[1\,0\,\bar{1}\,0]_p$
V2	$(1\,1\,1)_m//(0\,0\,0\,1)_p$	$[\bar{1}\,0\,1]_m//[1\,0\,\bar{1}\,0]_p$
V3	$(1\,1\,1)_m//(0\,0\,0\,1)_p$	$[0\,\bar{1}\,1]_m//[1\,0\,\bar{1}\,0]_p$
V4	$(\bar{1}\,1\,1)_m//(0\,0\,0\,1)_p$	$[\bar{1}\,\bar{1}\,0]_m//[1\,0\,\bar{1}\,0]_p$
V5	$(\bar{1}\,1\,1)_m//(0\,0\,0\,1)_p$	$[0\,\bar{1}\,1]_m//[1\,0\,\bar{1}\,0]_p$
V6	$(\bar{1}\,1\,1)_m//(0\,0\,0\,1)_p$	$[1\,0\,1]_m//[1\,0\,\bar{1}\,0]_p$
V7	$(\bar{1}\,1\,1)_m//(0\,0\,0\,1)_p$	$[\bar{1}\,1\,0]_m//[1\,0\,\bar{1}\,0]_p$
V8	$(\bar{1}\,1\,1)_m//(0\,0\,0\,1)_p$	$[\bar{1}\,0\,1]_m//[1\,0\,\bar{1}\,0]_p$
V9	$(\bar{1}\,1\,1)_m//(0\,0\,0\,1)_p$	$[0\,1\,1]_m//[1\,0\,\bar{1}\,0]_p$
V10	$(\bar{1}\,1\,1)_m//(0\,0\,0\,1)_p$	$[\bar{1}\,\bar{1}\,0]_m//[1\,0\,\bar{1}\,0]_p$
V11	$(\bar{1}\,1\,1)_m//(0\,0\,0\,1)_p$	$[0\,1\,1]_m//[1\,0\,\bar{1}\,0]_p$
V12	$(\bar{1}\,1\,1)_m//(0\,0\,0\,1)_p$	$[1\,0\,1]_m//[1\,0\,\bar{1}\,0]_p$

Downloaded by [Dartmouth College Library] at 05:54 01 December 2015

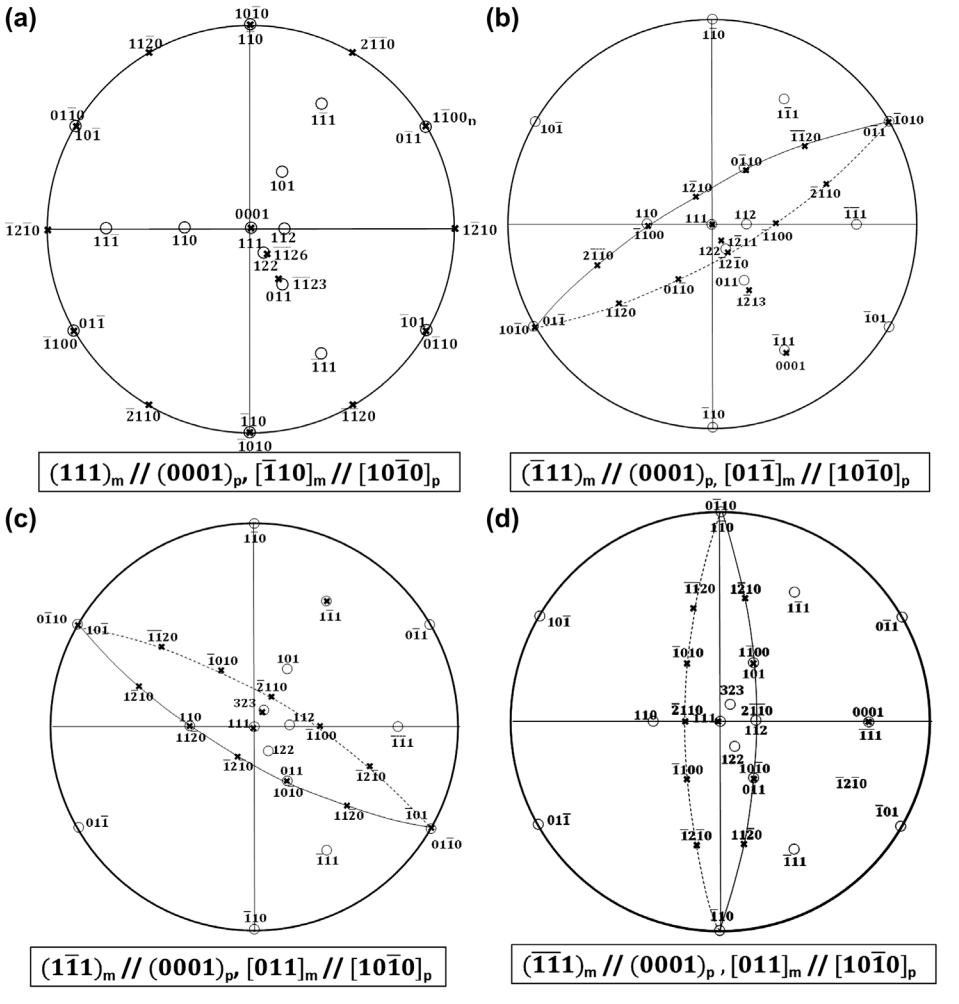

Figure 7. Superimposed stereographic projections of the four Laves and f.c.c. phase orientation variants observed in Fe–20Cr–30Ni–2Nb–5Al after ageing for 1325 h at 800 °C. (a) $(1\,1\,1)_m//(0\,0\,0\,1)_p$, $[\bar{1}\,1\,0]_m//[1\,0\,\bar{1}\,0]_p$; (b) $(\bar{1}\,1\,1)_m//(0\,0\,0\,1)_p$, $[0\,1\,\bar{1}]_m//[1\,0\,\bar{1}\,0]_p$; (c) $(1\,\bar{1}\,1)_m//(0\,0\,0\,1)_p$, $[0\,1\,1]_m//[1\,0\,\bar{1}\,0]_p$ (d) $(\bar{1}\,\bar{1}\,1)_m//(0\,0\,0\,1)_p$, $[0\,1\,1]_m//[1\,0\,\bar{1}\,0]_p$.

$$(\bar{1}\,\bar{1}\,1)_m//(0\,0\,0\,1)_p,\ [0\,1\,1]_m//[1\,0\,\bar{1}\,0]_p. \tag{4}$$

Based on the observation that for any given particle, the Laves phase {0 0 0 1} close-packed planes tend to align with the {1 1 1} close-packed planes of the matrix, it can be predicted that considering symmetry, the four {1 1 1} planes in the f.c.c. matrix, and the three ⟨1 1 0⟩ directions within each {1 1 1} plane, up to 12 variants of the Laves phase and matrix-orientation relationship might be observed in TEM studies (Table 2).

Figure 7 shows the superimposed stereographic projection of the Laves phase and matrix orientations. Since for directions of type ⟨0 0 0 1⟩ and ⟨h k i 0⟩ plane normal and directions have the same indices, only these directions are plotted on the stereograph.

Downloaded by [Dartmouth College Library] at 05:54 01 December 2015

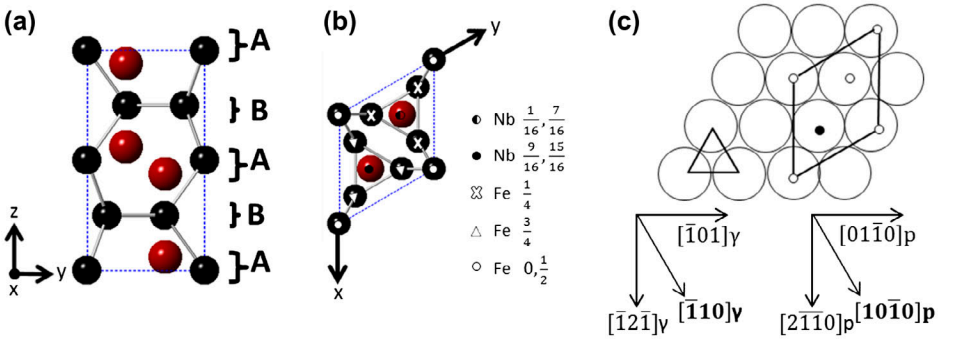

Figure 8. (colour online) (a) The AB stacking scheme of the C14 Laves phase structure of Fe2Nb as viewed down [0 0 0 1]; (b) Laves phase structure; (c) A Fe2Nb unit cell superimposed on a (1 1 1) matrix plane showing coherency between the basal plane atoms making up the 'A' triple layer and the matrix (slightly modified images from Denham and Silcock illustrations [43]).

Downloaded by [Dartmouth College Library] at 05:54 01 December 2015

$\{1\,0\,\bar{1}\,0\}$ and $\{1\,1\,\bar{2}\,0\}$ refer to prism planes of type I and type II, respectively [53]. Figure 7(a–d) shows the stereographic projections of the four variants described above with Laves phase (0 0 0 1) traces. The Laves phase $\{0\,0\,0\,1\}$ traces overlap with the matrix $\{1\,1\,1\}$ traces.

Particles with a hexagonal shape had the first orientation described above, while those that were more elongated and often plate-like and faceted are seen to grow along the other matrix $\{1\,1\,1\}$ directions. The calculated diffraction patterns of Figures 4(c), 5(d, e) and 6(c), $\{0\,0\,0\,1\}$ Laves and $\{1\,1\,1\}$ matrix planes are in close proximity to one another, and taken alone, this would suggest that these planes are nearly parallel and that $\langle 1\,1\,1\rangle$ are preferred directions for precipitate growth.

This observed orientation, according to Denham and Silcock is thought to be governed by the Fe and Nb containing *A*-layer of the Fe_2Nb (AB_2) and the attainment of the same atomic site densities for the matrix and precipitate [43]. In their description of the Laves Fe_2Nb structure, Fe atoms occupy the corner sites of the C14 unit cell. The stacking sequence along the 'c' axis is described as *ABAB* (Figure 8(a)), and the *A* layer is a puckered layer that consists of Nb and Fe with the Nb atoms at $\pm\frac{1}{16}z$, while the *B* layer contains Fe atoms (Figure 8(b)) [43]. The first layer of atoms that make up the basal plane of the Laves phase is coherent with the (1 1 1) matrix plane (Figure 8(c)) which results in a favourably small mismatch in lattice spacing. In their analysis, Denham and Silcock note that if a different orientation relationship occurred where the *B* layer of iron atoms were coherent instead, the density of atomic sites in the expanded matrix lattice would be 33% greater than in the observed orientation, which leads to the conclusion that it is the density relationship as well as the niobium atoms' role in nucleation at the reaction front that are the major factors that cause the orientation that is observed. Following the analysis in [43], given the above orientation relationship the f.c.c. matrix contracts by 6% in the $\langle 1\,1\,1\rangle$ direction and expands by 9% in the $\langle 1\,1\,2\rangle$ direction and the volume expansion on transformation from matrix to precipitate is 12%. As noted by [54] others have successfully concluded the preferred direction of precipitate growth following this methodology, but this is not always an accurate assumption. As predicted by the author in

Downloaded by [Dartmouth College Library] at 05:54 01 December 2015

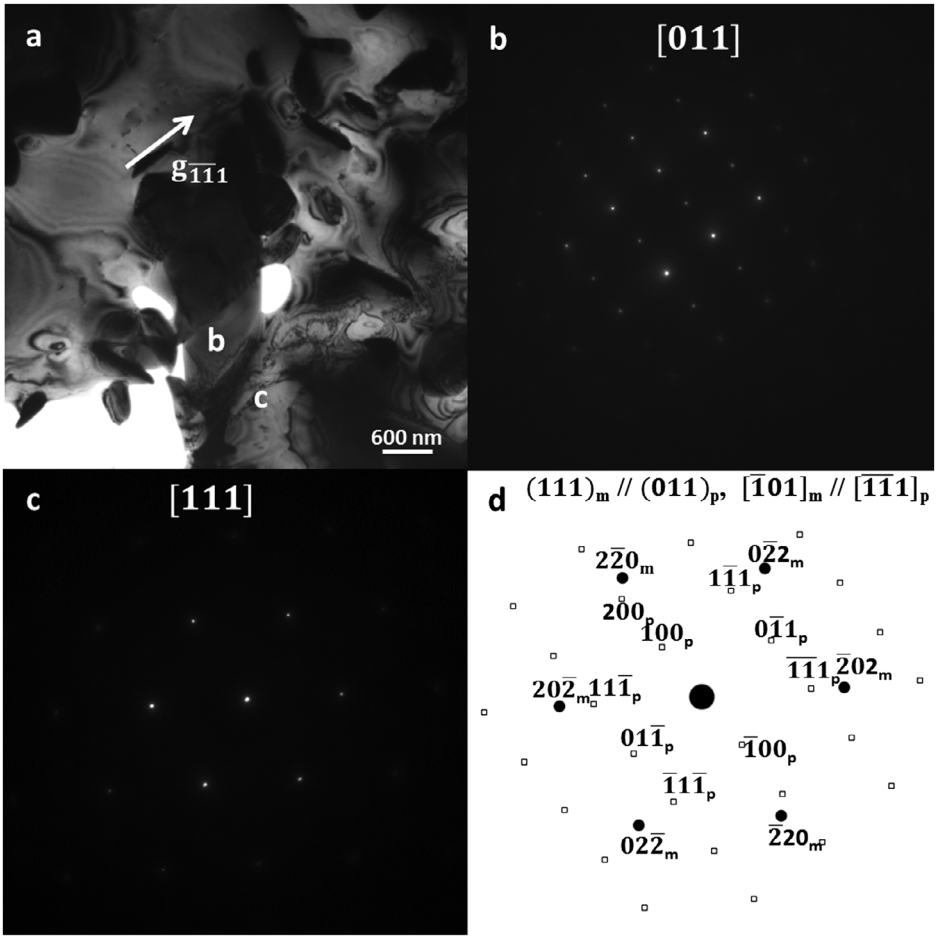

Figure 9. (a) A bright-field TEM image of a B2-NiAl particle with a typical K–S relationship; (b) SADP from the B2-NiAl particle with [0 1 1] zone axis; (c) selected area electron diffraction pattern from the f.c.c. matrix at [0 1 1]; (d) Schematic representation with indexing of *c* and *d* for the B2-NiAl particle having an OR of $(1\,1\,1)_m//(0\,1\,1)_p$, $[\bar{1}\,0\,1]_m//[\bar{1}\,\bar{1}\,1]_p$.

[18] and much like in [43] the Laves phase in the orientation relationship that has been observed was determined to have only a moderate misfit with the austenite matrix. This may help to explain why this alloy has been shown to have room temperature ductility despite the presence of these brittle precipitates.

NiAl and matrix-orientation relationship

Figure 9(a) shows a bright-field TEM image of a B2-NiAl particle. Figure 9(b) and (c) show a SADP taken from the NiAl particle and matrix, respectively. In Figure 9(b), the particle is tilted to [0 1 1] and the matrix in coincident [1 1 1] in Figure 9(c). Figure 9(d) is a schematic of a superimposed diffraction pattern of both the particle and matrix. From the diffraction pattern the particle was concluded to have a $(1\,1\,1)_m//(0\,1\,1)_p$,

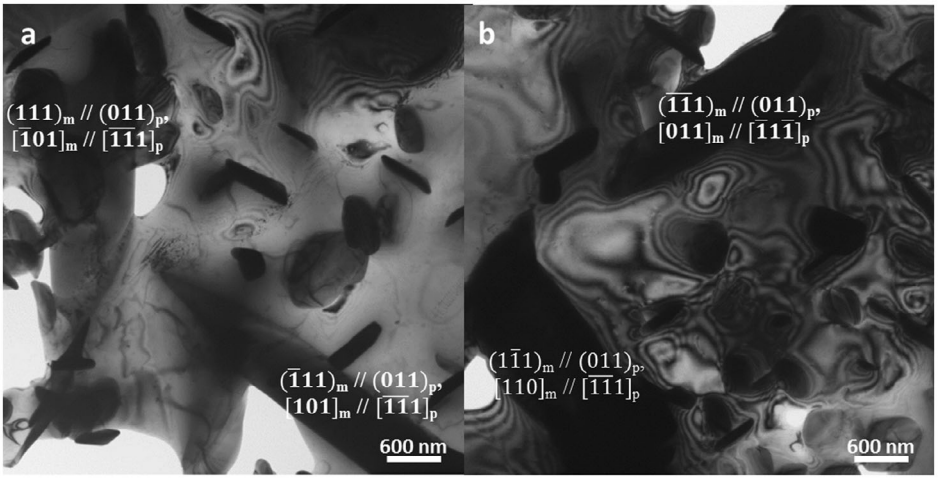

Figure 10. TEM bright-field image showing B2-NiAl particles displaying four variants of the K–S-orientation relationship.

$[\bar{1}\,0\,1]_m//[\overline{1\,1}\,1]_p$ orientation relationship, which is consistent with the Kurdjumov–Sachs-orientation relationship.

Figure 10 shows bright-field TEM images of additional B2-NiAl particles exhibiting different Kurdjumov–Sachs-orientation variants determined via tilting experiments in the TEM. In Figure 10(a), one additional NiAl particle Kurdjumov–Sachs variant is observed (to the right of the particle from Figure 9). It was determined to have the orientation relationship $(\bar{1}\,1\,1)_m//(0\,1\,1)_p$, $[1\,0\,1]_m//[\overline{1\,1}\,1]_p$. In Figure 10(b), two B2-NiAl particles and shown with $(1\,\bar{1}\,1)_m//(0\,1\,1)_p$, $[1\,1\,0]_m//[\overline{1\,1}\,1]_p$, and $(\overline{1\,1}\,1)_m//(0\,1\,1)_p$, $[0\,1\,1]_m//[\bar{1}\,1\,\bar{1}]_p$ variants of the Kurdjumov–Sachs relationship.

Unlike with the Laves phase, NiAl particles that appeared to be oriented similarly in bright-field TEM images were observed to occasionally represent different variants of the K–S relationship. For example, Figure 11 shows an analysis of two nearly side-by-side B2-NiAl particles in the matrix. Figure 11(a) is a bright-field TEM image of the two particles in the matrix. Figure 11(b) shows a diffraction from the matrix down the [3 2 3] zone axis. Figure 11(c) and (d) show the diffraction patterns from the two NiAl particles while the matrix is at the [3 2 3] axis. Figure 11(e) and (f) show the simulated diffraction patterns of the two particles. Though the particles appear to be oriented in the same direction based on the TEM bright-field image, their respective diffraction patterns reveal that they are two distinct twin-related variants of the K–S relationship having orientations of $(1\,\bar{1}\,1)_m//(0\,1\,1)_p$, $[1\,0\,\bar{1}]_m//[\overline{1\,1}\,1]_p$, and $(1\,\bar{1}\,1)_m//(0\,1\,1)_p$, $[1\,0\,\bar{1}]_m//[\bar{1}\,1\,\bar{1}]_p$, respectively.

In studies of the morphology and crystallography of martensite in steels a total of 24 (V1–V24) possible variants have been predicted for the K–S relationship [55–57]. Figure 12 shows the superimposed stereographic projections of the matrix and B2-NiAl particles that have the K–S relationship. {1 1 1} and {0 1 1} matrix and precipitate planes are plotted on the stereographic projections. In this study, a total of six of the 24 K–S variants were observed:

Downloaded by [Dartmouth College Library] at 05:54 01 December 2015

Downloaded by [Dartmouth College Library] at 05:54 01 December 2015

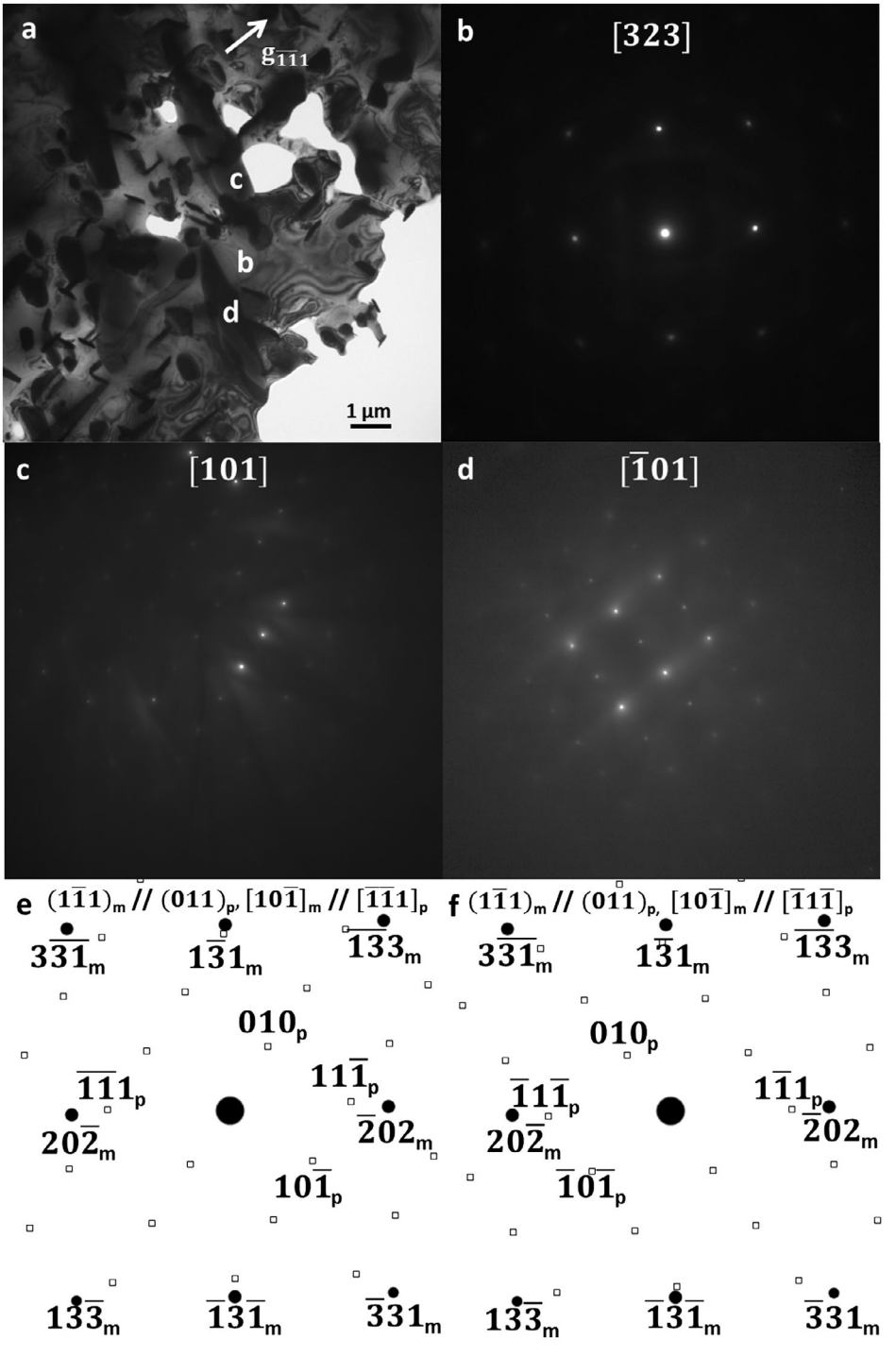

Figure 11. (a) A bright-field TEM image showing two variants of the B2-NiAl phase in an f.c.c. matrix; (b) selected area electron diffraction pattern from the f.c.c. matrix at [3 2 3]; (c and d) SADP from the two B2-NiAl particles with [1 0 1] and [$\bar{1}$ 0 1] zone axes, respectively, (e and f) schematic representation of the orientation relationship observed for (c and d), $(1\,\bar{1}\,1)_m//(0\,1\,1)_p$, $[1\,0\,\bar{1}]_m//[\bar{1}\,\bar{1}\,1]_p$, and $(1\,\bar{1}\,1)_m//(0\,1\,1)_p$, $[1\,0\,\bar{1}]_m//[\bar{1}\,1\,\bar{1}]_p$, respectively, with indexing.

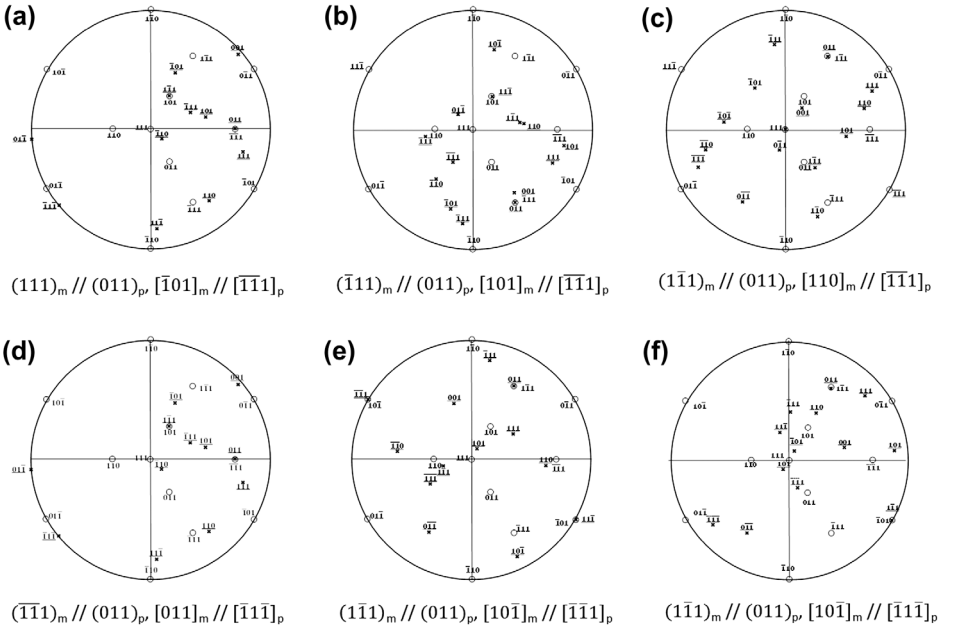

Figure 12. Superimposed stereographic projections of the six variants of the B2-NiAl and f.c.c. K–S-orientation relationship observed showing {1 1 1}, and {0 1 1} planes. (a) $(1\,1\,1)_m//(0\,1\,1)_p$, $[\bar{1}\,0\,1]_m//[\bar{1}\,\bar{1}\,1]_p$; (b) $(\bar{1}\,1\,1)_m//(0\,1\,1)_p$, $[1\,0\,1]_m//[\bar{1}\,\bar{1}\,1]_p$; (c) $(1\,\bar{1}\,1)_m//(0\,1\,1)_p$, $[1\,1\,0]_m//[\bar{1}\,\bar{1}\,1]_p$; (d) $(\bar{1}\,\bar{1}\,1)_m//(0\,1\,1)_p$, $[0\,1\,1]_m//[\bar{1}\,1\,\bar{1}]_p$; (e) $(1\,\bar{1}\,1)_m//(0\,1\,1)_p$, $[1\,0\,\bar{1}]_m//[\bar{1}\,\bar{1}\,1]_p$; (f) $(1\,\bar{1}\,1)_m//(0\,1\,1)_p$, $[1\,0\,\bar{1}]_m//[\bar{1}\,1\,\bar{1}]_p$.

$$(V1) : (1\,1\,1)_m//(0\,1\,1)_p, [\bar{1}\,0\,1]_m//[\bar{1}\,\bar{1}\,1]_p, \tag{5}$$

$$(V11) : (\bar{1}\,1\,1)_m//(0\,1\,1)_p, [1\,0\,1]_m//[\bar{1}\,\bar{1}\,1]_p, \tag{6}$$

$$(V13) : (1\,\bar{1}\,1)_m//(0\,1\,1)_p, [1\,1\,0]_m//[\bar{1}\,\bar{1}\,1]_p, \tag{7}$$

$$(V24) : (\bar{1}\,\bar{1}\,1)_m//(0\,1\,1)_p, [0\,1\,1]_m//[\bar{1}\,1\,\bar{1}]_p, \tag{8}$$

$$(V7) : (1\,\bar{1}\,1)_m//(0\,1\,1)_p, [1\,0\,\bar{1}]_m//[\bar{1}\,\bar{1}\,1]_p, \tag{9}$$

$$(V8) : (1\,\bar{1}\,1)_m//(0\,1\,1)_p, [1\,0\,\bar{1}]_m//[\bar{1}\,1\,\bar{1}]_p. \tag{10}$$

Others have noted K–S variants and theory suggest that the lattice parameter value plays an important role in the determination of the preferred orientation observed in f.c.c./b.c.c. systems. The K–S-orientation relationship has been seen in an FNCA alloy [30,31] with B2-NiAl precipitates that also had a plate-like morphology. In that case, two K–S-orientation relationship variants were observed. In a study of f.c.c. Co precipitates in a B2-ordered (Ni, Co)Al alloy [58], three variants of the K–S-orientation relationship were observed and it was noted that the ratio of the lattice parameters of the

Downloaded by [Dartmouth College Library] at 05:54 01 December 2015

f.c.c and b.c.c. phase can influence the orientation relationship. In [54] it was predicted that b.c.c. and f.c.c. systems have a lattice parameter ratio between 1.21 and 1.36 would have the K–S relationship. Given the value of 1.25 for the lattice parameter ratio between the f.c.c. matrix and the B2-NiAl in this alloy, it is not surprising that Kx2013; S-orientation is observed for the NiAl precipitates.

Conclusions

Hexagonal-shaped and elongated Fe_2Nb-type Laves phase, and plate-like B2-NiAl precipitates were observed after a solution anneal at 1250 °C followed by ageing at 800 °C in Fe–20Cr–30Ni–2Nb–5Al. The orientation between the f.c.c. matrix and Laves phase was determined to have the $(1\,1\,1)_m//(0\,0\,0\,1)_p$, $[\bar{1}\,1\,0]_m//[1\,0\,\bar{1}\,0]_p$ orientation relationship proposed by Denham and Silcock. The B2-NiAl precipitates were determined to have a Kurdjumov–Sachs-orientation relationship with the matrix, i.e. $(1\,1\,1)_m//(0\,1\,1)_p$, $[\bar{1}\,0\,1]_m//[\overline{1\,1}\,1]_p$. While the Laves phase particles primarily followed four variants, six variants of the K–S-orientation were observed for the B2-NiAl particles.

Acknowledgements

This research was supported by the National Science Foundation Grant DMR 1206240. Any opinions, findings, conclusions or recommendations expressed in this material are those of the author (s) and do not necessarily reflect the views of the National Science Foundation. Dr Easo P. George is thanked for the casting of the alloy.

Disclosure statement

No potential conflict of interest was reported by the authors.

Funding

This work was supported by Division of Materials Research [1206240].

References

[1] M.P. Brady, J. Magee, Y. Yamamoto, D. Helmick and L. Wang, Mater. Sci. Eng., A 590 (2014) p.101.
[2] P. Kofstad, Oxid. Met. 44 (1995) p.3.
[3] U. Heubner, *Nickel Alloys*, CRC Press, New York, 2000.
[4] J.A. McGurty, *Austenitic Iron Alloys*, US Patent No. 4,086,085, April 1978.
[5] Y. Yamamoto, M.P. Brady, Z.P. Lu, P.J. Maziasz, C.T. Liu, B.A. Pint, K.L. More, H.M. Meyer and E.A. Payzant, Science 316 (2007) p.433.
[6] M.P. Brady, Y. Yamamoto, M.L. Santella, P.J. Maziasz, B.A. Pint, C.T. Liu, Z.P. Lu and H. Bei, JOM 60 (July 2008) p.12.
[7] Y. Yamamoto, M. Takeyama, Z.P. Lu, C.T. Liu, N.D. Evans, P.J. Maziasz and M.P. Brady, Intermetallics 16 (2008) p.453.
[8] Y. Yamamoto, M.P. Brady, M.L. Santella, H. Bei, P.J. Maziasz and B.A. Pint, Metall. Mater. Trans. A 42 (2011) p.922.
[9] Y. Yamamoto, M.P. Brady, Z.P. Lu, C.T. Liu, M. Takeyama, P.J. Maziasz and B.A. Pint, Metall. Mater. Trans. A 38 (2007) p.2737.

Downloaded by [Dartmouth College Library] at 05:54 01 December 2015

[10] M.P. Brady, Y. Yamamoto, M.L. Santella and B.A. Pint, Scr. Mater. 57 (2007) p.1117.
[11] Y. Yamamoto, M.L. Santella, M.P. Brady, H. Bei and P.J. Maziasz, Metall. Mater. Trans. A 40 (2009) p.1868.
[12] M.P. Brady, Y. Yamamoto, M.L. Santella and L.R. Walker, Oxid. Met. 72 (2009) p.311.
[13] M.P. Brady, Y. Yamamoto, B.A. Pint, M.L. Santella, P.J. Maziasz and L.R. Walker, *On the loss of protective scale formation in creep-resistant, alumina-forming austenitic stainless steels at 900 C in air*, in *Materials Science Forum*, P. Steinmetz, I.G. Wright, A. Galerie, D. Monceau and S. Mathieu, eds., Trans Tech Publ, Zurich, 2008, p.725.
[14] Y. Yamamoto, M.L. Santella, C.T. Liu, N.D. Evans, P.J. Maziasz and M.P. Brady, Mater. Sci. Eng., A 524 (2009) p.176.
[15] H. Bei, Y. Yamamoto, M.P. Brady and M.L. Santella, Mater. Sci. Eng., A 527 (2009) p.2079.
[16] M.P. Brady, K.A. Unocic, M.J. Lance, M.L. Santella, Y. Yamamoto and L.R. Walker, Oxid. Met. 75 (2011) p.337.
[17] Y. Yamamoto, G. Muralidharan and M.P. Brady, Scr. Mater. 69 (2013) p.816.
[18] G. Trotter and I. Baker, Mater. Sci. Eng., A 627 (2015) p.270.
[19] G. Trotter, G. Rayner, I. Baker and P.R. Munroe, Intermetallics 53 (2014) p.120.
[20] D.Q. Zhou, X.Q. Xu, H.H. Mao, Y.F. Yan, T.G. Nieh and Z.P. Lu, Mater. Sci. Eng., A 594 (2014) p.246.
[21] S.W. Chen, C. Zhang, Z.X. Xia, H. Ishikawa and Z.G. Yang, Mater. Sci. Eng., A 616 (2014) p.183.
[22] M. Takeyama, Mater. Sci. Forum 539–543 (2007) p.3012.
[23] T. Koutsoukis, A. Redjaïmia and G. Fourlaris, Mater. Sci. Eng., A 561 (2013) p.477.
[24] K.S. Kumar and P.M. Hazzledine, Intermetallics 12 (2004) p.763.
[25] K.S. Kumar, L. Pang, C.T. Liu, J. Horton and E.A. Kenik, Acta Mater. 48 (2000) p.911.
[26] J. Aufrecht, A. Leineweber, V. Duppel and E.J. Mittemeijer, Intermetallics 19 (2011) p.1428.
[27] J. Aufrecht, A. Leineweber and E.J. Mittemeijer, Intermetallics 19 (2011) p.1442.
[28] S. Heino, Metall. Mater. Trans. A 31 (2000) p.1893.
[29] P.W. Hochanadel, G.R. Edwards, C.V. Robino and M.J. Cieslak, Metall. Mater. Trans. A 25 (1994) p.789.
[30] D.V.V. Satyanarayana, G. Malakondaiah and D.S. Sarma, Mater. Sci. Eng., A 323 (2002) p.119.
[31] D.V.V. Satyanarayana, G. Malakondaiah and D.S. Sarma, Mater. Charact. 47 (2001) p.61.
[32] A. Bhowmik, S. Neumeier, J.S. Barnard, C.H. Zenk, M. Göken, C.M. Rae and H.J. Stone, Phil. Mag. 94 (2014) p.3914.
[33] A. Bhowmik, H.T. Pang, I.M. Edmonds, C.M.F. Rae and H.J. Stone, Intermetallics 32 (2013) p.373.
[34] A. Bhowmik and H. Stone, J. Mater. Sci. 48 (2013) p.3283.
[35] A. Bhowmik, C.N. Jones, I.M. Edmonds and H.J. Stone, J. Alloys Compd. 530 (2012) p.169.
[36] A. Bhowmik, K.M. Knowles and H.J. Stone, Intermetallics 31 (2012) p.34.
[37] A. Bhowmik, H.T. Pang, S. Neumeier, H.J. Stone and I. Edmonds, MRS Online Proc. Library 1295 (2011) p.323.
[38] K. Kumar, MRS Proc. 460 (1996) p.677.
[39] K.S. Kumar and P.M. Hazzledine, MRS Proc. 364 (1994) p.1383.
[40] K.S. Kumar and D.B. Miracle, Intermetallics 2 (1994) p.257.
[41] A.F. Padilha, I.F. Machado and R.L. Plaut, J. Mater. Process. Technol. 170 (2005) p.89.
[42] M. Takeyama, N. Gomi, S. Morita and T. Matsuo, MRS Online Proc. Library 842 (2004) p.S5.37.1.
[43] A. Denham and J. Silcock, J. Iron Steel Inst. 207 (1969) p.582.
[44] M.J. Cooper, Phil. Mag. 8 (1963) p.805.

Downloaded by [Dartmouth College Library] at 05:54 01 December 2015

[45] H. Xiao and I. Baker, Acta Metall. Mater. 42 (1994) p.1535.
[46] R. Schnitzer, R. Radis, M. Nöhrer, M. Schober, R. Hochfellner, S. Zinner, E. Povoden-Karadeniz, E. Kozeschnik and H. Leitner, Mater. Chem. Phys. 122 (2010) p.138.
[47] N. Takata, H. Ghassemi-Armaki, Y. Terada, M. Takeyama and K.S. Kumar, Scr. Mater. 68 (2013) p.615.
[48] S. Ishikawa, T. Matsuo and M. Takeyama, MRS Fall Meeting. 2008 (2008) p. 1.
[49] Y. Komura, Acta Crystallogr. 15 (1962) p.770.
[50] W. Kim, S. Hong and K. Lee, Met. Mater. Int. 16 (2010) p.171.
[51] C. Allen, P. Delavignette and S. Amelinckx, Phys. Status Solidi A 9 (1972) p.237.
[52] X.-Q. Chen, W. Wolf, R. Podloucky, P. Rogl and M. Marsman, Europhys. Lett. 67 (2004) p.807.
[53] P.G. Partridge, Metall. Rev. 12 (1967) p.169.
[54] U. Dahmen, Acta Metall. 30 (1982) p.63.
[55] E. Pereloma and D.V. Edmonds, *Phase Transformations in Steels: Diffusionless Transformations, High Strength Steels, Modelling and Advanced Analytical Techniques*, Vol. 2, Elsevier, Sawston, 2012.
[56] S. Morito, H. Tanaka, R. Konishi, T. Furuhara and T. Maki, Acta Mater. 51 (2003) p.1789.
[57] S. Morito, Y. Adachi and T. Ohba, Mater. Trans. 50 (2009) p.1919.
[58] W.H. Tian, M. Hibino and M. Nemoto, Intermetallics 6 (1998) p.121.

Downloaded by [Dartmouth College Library] at 05:54 01 December 2015